

Signature of quantum interference upon sudden ionization and excitation of an electronic wavepacket in fluoro-benzene

Anthony Ferté,¹ João Pedro Malhado,² and Morgane Vacher^{1,*}

¹*Nantes Université, CNRS, CEISAM, UMR 6230, F-44000 Nantes, France*

²*Chemistry Department, Imperial College London,*

Prince Consort Road, London, SW7 2AZ, UK

(Dated: September 18, 2023)

Ultrashort pulses can excite or ionize molecules and populate coherent electronic wavepackets, controlling the induced dynamics. In this letter, we simulate the quantum coupled electron-nuclear dynamics in full dimensionality upon ionization to different electronic wavepackets of benzene and fluoro-benzene molecules. In fluoro-benzene, the calculations unravel both inter-state and intra-state quantum interferences that leave clear signatures in the shape of the autocorrelation function. The latter could be measured experimentally via high harmonic spectroscopy.

With ultrashort light pulse sources emerging [1, 2], the time resolution of measurements is pushed to the intrinsic timescale of electron dynamics in molecules *i.e.* the attosecond [3–6]. Exploiting the large pulse bandwidth to coherently excite several electronic states, and forming a so-called electronic wavepacket [7–9], unveiled the prospect to go beyond the possibilities of standard photochemistry. Indeed, one can in principle use the interference between the components of the electronic wavepacket to steer chemical reactivity. Such attochemical control, also called charge-directed reactivity, was demonstrated theoretically and experimentally in diatomics [10, 11]. Extending it to polyatomic molecules is one of the current main prospects of attochemistry [12, 13].

From the experimental point of view, generating and observing such dynamics is challenging. Attosecond pump-attosecond probe schemes, although becoming possible [14–17], are arduous. As an alternative, high-harmonic generation spectroscopy (HHS) [18] has been successfully applied to probe the sub-femtosecond coupled electron-nuclear dynamics on simple systems, retrieving autocorrelation functions [19–26]. Its main disadvantage is that the measurement is performed in the presence of a strong field that may perturb the dynamics to be studied. Recent developments of this method allowed to measure the dynamics in polyatomic molecules [27].

From a theoretical perspective, simulating a chemical reaction induced by an electronic wavepacket is also challenging. Most calculations attempting it either were performed with fully quantum dynamics methods but limited to small molecules [28, 29] or medium-size molecules but in reduced-dimensionality [30, 31], or employed mixed quantum-classical dynamics methods [32–35]. The models used in fully quantum dynam-

ics simulations are mostly suited to describe rigid motions and are thus difficult to apply to reactions such as dissociations or *cis-trans* isomerisations. On the other hand, reduced dimensionality may yield misleading results by not capturing all relevant features of the dynamics. Finally, mixed quantum-classical dynamics methods do not treat electronic coherence accurately. Yet, electronic coherence is key to attochemistry.

In this letter, the coupled electron-nuclear dynamics upon ionization and excitation of electronic wavepackets in benzene derivatives (Fig. 1) is simulated fully quantum mechanically and in full dimensionality. The calculations show that, upon population of different superpositions of the two lowest cationic states of fluoro-benzene, several types of quantum interferences leave clear signatures in the autocorrelation function, a quantity accessible experimentally *via* HHS [27].

Benzene (BZ) and its derivatives are a formidable set of systems to investigate quantum coupled electron-nuclear dynamics induced upon ionization by attosecond/sub-femtosecond pulses [34, 36, 37]. Indeed, vertical ionization of the benzene molecule leads exactly to the conical intersection between the two lowest doublet cationic states of *quinoid* (Ψ_Q) and *anti-quinoid* (Ψ_A) characters. The reduced symmetry of the fluoro-benzene (FBZ) in-

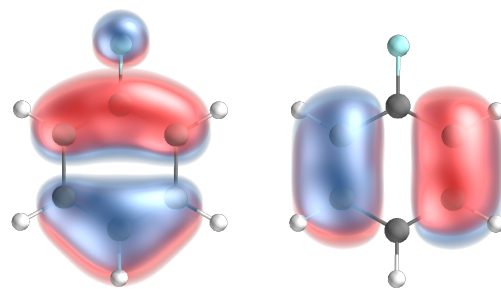


FIG. 1: Singly occupied molecular orbitals (SOMO) of the Ψ_Q (left) and Ψ_A (right) cationic states of FBZ.

*Electronic address: morgane.vacher@univ-nantes.fr

duces a slight offset between the neutral structure and the electronic degeneracy point in the cation, leading to a finite energy gap at the vertical ionization geometry: $\Delta E_{\text{vert.}}^{\text{adia.}} \approx 0.27$ eV.

Moreover, FBZ has a permanent dipole moment of 1.66 D and its two lowest cationic states are characterized by orthogonal transition dipole moments due to the electron being ejected from orbitals with perpendicular nodal planes (see Fig. 1). Thus, by first aligning the neutral target with an electric field and modulating the angle of the ionizing pulse polarization, one can experimentally control the relative weight of the two coherently populated electronic states [38, 39]. Therefore, these systems offer a unique opportunity to investigate the dynamics of different types of electronic wavepackets, before electronic decoherence [40–47].

In previous works based on mixed quantum-classical simulations, one of the present author demonstrated that upon ionization of benzene and toluene, the composition of the electronic wavepacket rules over the molecular motion induced in the branching space associated with the nearby conical intersection [32, 48]. If mixed quantum-classical simulations can recover average nuclear motions, one major limitation is that describing purely quantum effects is out of reach.

In the present full quantum mechanical simulations of the post-ionization coupled electron-nuclear dynamics of BZ, deuterated BZ, and FBZ, several initial electronic wavepackets were considered: the pure diabatic states, Ψ_Q and Ψ_A , as well as both equally weighted, real-valued, in-phase and opposite-phase superpositions *i.e.* $\frac{1}{\sqrt{2}}(\Psi_Q \pm \Psi_A)$. The dynamics was simulated using the single-set formalism of the Direct-Dynamics variational Multi-Configurational Gaussian (DD-vMCG) method, as implemented in the Quantics package [49]: the molecular wavepacket is expanded onto a set of variationally coupled time-dependent Gaussian basis functions (GBF) that evolve quantum mechanically [50–52]. The post-ionization dynamics of (deuterated) BZ and FBZ molecules were simulated for 10 fs using 5 and 10 GBF respectively, to achieve convergence (see Fig. 8 in SI). Electronic structure calculations were performed at the CASSCF(5e, 6o) level *via* the Gaussian software [53] with an active space including the π/π^* orbitals and using the 6-31G* basis set. Electronic state diabatization was performed using the regularization method [54, 55].

Figure 2 shows the resulting average nuclear motion *i.e.* the expectation value of the nuclear position in the branching space of BZ and FBZ, induced by the different wavepackets considered. For both systems, populating a pure diabatic state leads to an initial motion oriented solely along the gradient difference vector with opposite directions

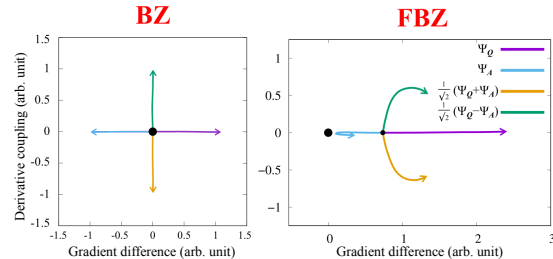


FIG. 2: Average quantum nuclear motion in the branching space over 10 fs and upon ionization of BZ (left) and FBZ (right) molecules and upon initial population of Ψ_Q (purple), Ψ_A (blue), $\frac{1}{\sqrt{2}}(\Psi_Q + \Psi_A)$ (orange) and $\frac{1}{\sqrt{2}}(\Psi_Q - \Psi_A)$ (green). The large black circle indicates the conical intersection point while the small black circle marks the vertical ionization geometry (superimposed in BZ).

(see Fig. 7 in S.I. for a representation of the branching space vectors). On the other hand, population of mixed superpositions, $\frac{1}{\sqrt{2}}(\Psi_Q \pm \Psi_A)$, leads to an initial average motion mostly oriented along the derivative coupling vector, again with opposite directions. Unsurprisingly, as only the π conjugated system is involved in the ionization and excitation processes investigated, the subsequent nuclear motion almost only involve the carbon ring. As a result, the BZ and deuterated BZ display highly similar dynamics (see Fig. 9 in SI). These observations are in line with the previous mixed quantum-classical [32, 48] and quantum [56] simulations, validating the control over the molecular motion in the branching space achieved by tuning the initial electronic wavepacket composition.

Initially, the induced average nuclear motions are qualitatively similar in BZ and FBZ. Two differences appear at “longer” times: (i) upon excitation of FBZ to the antiquinoid state, the molecular wavepacket first evolves towards the conical intersection and then turns back; (ii) upon excitation of FBZ to a mixed wavepacket, the molecule moves along the gradient difference as well. This indicates a richer dynamics in the case of FBZ, the detailed of which will be thoroughly discussed in an upcoming article.

The present letter focuses on the signature of quantum interferences in these dynamics. One key difference between BZ and FBZ is the following: In the BZ cation, both adiabatic states are degenerate at the neutral geometry. As a consequence, any superposition of the two electronic states is a valid eigenstate of the electronic Hamiltonian and thus, BZ is always excited to a pure adiabatic eigenstate preventing interferences between the two states. On the other hand, in FBZ, the two adiabatic states are not degenerate at the vertical ionization geometry and their coherent population can thus lead to quantum interferences.

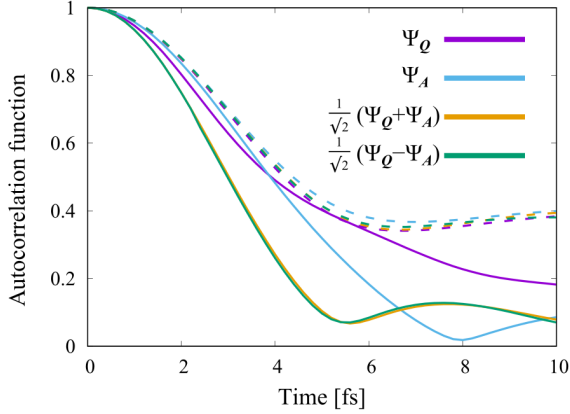


FIG. 3: Modulus of the autocorrelation functions along the quantum dynamics induced upon ionization of BZ (dashed) and FBZ (solid) molecules and excitation to Ψ_Q (purple), Ψ_A (blue), $\frac{1}{\sqrt{2}}(\Psi_Q + \Psi_A)$ (orange) and $\frac{1}{\sqrt{2}}(\Psi_Q - \Psi_A)$ (green) electronic wavepackets.

Here, we search for such effects in the autocorrelation function,

$$\mathcal{O}(t) = \langle \Psi^{\text{mol}}(0) | \Psi^{\text{mol}}(t) \rangle, \quad (1)$$

the overlap between the molecular wavepacket Ψ^{mol} at time t and at $t = 0$ *i.e.* the ionization time. Figure 3 reports the autocorrelation functions for both BZ and FBZ molecules, upon excitation to the different electronic wavepackets considered. The initial evolution of these autocorrelation functions was fitted using a Gaussian expression, $\exp(-(t/\tau)^2/2)$. The corresponding decay times, τ , are reported in Table I.

TABLE I: Decay times τ deduced from the fits of the early time evolution of the autocorrelation functions, upon ionization of BZ and FBZ molecules and initial population of Ψ_Q , Ψ_A , and $\frac{1}{\sqrt{2}}(\Psi_Q \pm \Psi_A)$ electronic wavepackets.

	Ψ_Q	Ψ_A	$\frac{1}{\sqrt{2}}(\Psi_Q + \Psi_A)$	$\frac{1}{\sqrt{2}}(\Psi_Q - \Psi_A)$
BZ	3.51 fs	3.56 fs	3.54 fs	3.55 fs
FBZ	3.05 fs	3.33 fs	2.64 fs	2.64 fs

In the case of the BZ molecule (dashed curves), all four initial electronic wavepackets yield very similar autocorrelation functions: it steadily decreases from 1 with a decay time of ≈ 3.5 fs, reaches a minimum value of about 0.4 around 6 fs and very slowly increases afterward. The absence of significant differences reflects the isotropy of the potential energy surfaces around the Ψ_Q/Ψ_A conical intersection. It also prevents one to deduce from the nuclear autocorrelation function, which electronic state was initially excited. Again, the shape and decay time of the autocorelation functions obtained for the deuterated BZ molecule are

very similar to those of BZ (see Fig. 9 in SI). For the BZ molecule, these predicted decay times are significantly longer than the sub-fs value reported in another work using an approximate approach to compute short-time autocorrelation functions near a conical intersection [57]. They are, however, in excellent agreement with the ($\tau = 4 \pm 1$ fs) value obtained by recent HHS measurements on BZ and deuterated BZ [27].

The FBZ results (solid curves) show a completely different picture. First, all electronic wavepackets yield autocorrelation functions that drop to significantly lower values, almost reaching 0 upon population of the higher lying (at the vertical geometry) Ψ_A diabatic state. In addition, to the exception of the two equally weighted superpositions that are indistinguishable due to the symmetry of the derivative coupling, the initially excited electronic wavepacket can easily be determined from the subsequent autocorrelation function and its decay time. Finally, a significantly faster decay is clearly observed in the case of the initially mixed electronic wavepackets: 2.6 fs instead of $3.0 - 3.3$ fs.

To understand further the faster decay of the autocorrelation function in the case of mixed electronic wavepackets, one can analyse in more details $\mathcal{O}^{Q+A}(t)$, the autocorrelation function of the FBZ molecule initially excited to $\frac{1}{\sqrt{2}}(\Psi_Q + \Psi_A)$. Since the system is in a superposition of the two diabatic states, the autocorrelation function is obtained as the coherent sum of two complex terms,

$$\mathcal{O}^{Q+A}(t) = \underbrace{\sum_{i,j} C_i^{Q*}(0) C_j^Q(t) \times \langle \mathcal{X}_i(0) | \mathcal{X}_j(t) \rangle}_{\mathcal{O}_Q^{Q+A}(t)} + \underbrace{\sum_{i,j} C_i^{A*}(0) C_j^A(t) \times \langle \mathcal{X}_i(0) | \mathcal{X}_j(t) \rangle}_{\mathcal{O}_A^{Q+A}(t)}, \quad (2)$$

where $C_i^{Q/A}(t)$ are the expansion coefficients of the molecular wavepacket on diabatic state “Q/A” and GBF $\mathcal{X}_i(t)$ at time t .

Figure 4 decomposes the full autocorrelation function $\mathcal{O}^{Q+A}(t)$ (orange), onto its two diabatic components thereafter $\mathcal{O}_Q^{Q+A}(t)$ (dashed purple) and $\mathcal{O}_A^{Q+A}(t)$ (dashed blue). Are also reported the interference-free incoherent sum $|\mathcal{O}_Q^{Q+A}(t)| + |\mathcal{O}_A^{Q+A}(t)|$ (black), and the complete autocorrelation function of the FBZ system upon initial population of the pure diabatic states here denoted $\mathcal{O}^Q(t)$ (purple) and $\mathcal{O}^A(t)$ (blue). Similar plots for the other mixed wavepackets and for the BZ molecule are presented in SI (see Fig. 10).

The naive incoherent summation of both diabatic components (black) yields a result very different from the true autocorrelation function (orange):

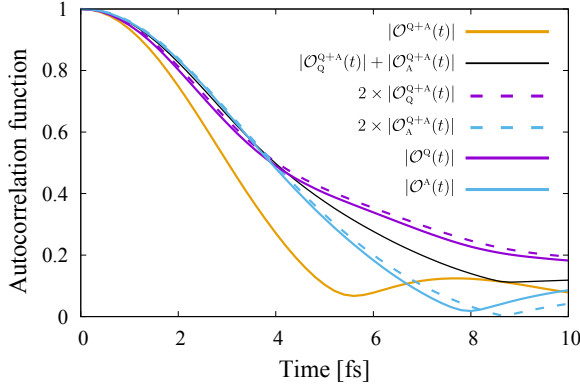


FIG. 4: Modulus of $\mathcal{O}^{Q+A}(t)$ the autocorrelation function of the FBZ cation upon initial population of the $\frac{1}{\sqrt{2}}(\Psi_Q + \Psi_A)$ wavepacket (orange) and of its two diabatic components $\mathcal{O}_Q^{Q+A}(t)$ (dashed purple) and $\mathcal{O}_A^{Q+A}(t)$ (dashed blue), note that they were doubled here for ease of representation. Incoherent sum $|\mathcal{O}_Q^{Q+A}(t)| + |\mathcal{O}_A^{Q+A}(t)|$ (black). Modulus of the autocorrelation functions of the FBZ cation upon initial population of a pure diabatic state, $\mathcal{O}^Q(t)$ (purple) and $\mathcal{O}^A(t)$ (blue).

slower decay with no structure. This demonstrates that interferences between the two diabatic components are responsible for the accelerated decay of the autocorrelation function of the FBZ system upon initial population of a mixed electronic wavepacket. This effect is named *inter-state interference* hereafter. Interestingly, the two diabatic components of the total autocorrelation function behave very similarly to those of the corresponding pure diabatic states. This may not be expected since the nuclear dynamics depends on the composition of the electronic wavepacket.

For both $\mathcal{O}_{Q/A}^{Q+A}(t)$ terms to interfere, a phase difference, $\Delta\varphi(t) = \arg(\mathcal{O}_Q^{Q+A}(t)) - \arg(\mathcal{O}_A^{Q+A}(t))$, with $\arg(X)$ being the argument of the complex number X , has to accumulate along the dynamics. Indeed, from Eq. (2) one easily obtains that

$$|\mathcal{O}^{Q+A}(t)|^2 = |\mathcal{O}_Q^{Q+A}(t)|^2 + |\mathcal{O}_A^{Q+A}(t)|^2 + |\mathcal{O}_Q^{Q+A}(t)| \times |\mathcal{O}_A^{Q+A}(t)| \times 2 \cos(\Delta\varphi(t)). \quad (3)$$

Importantly, this phase difference is independent of the initial (absolute or relative) phases of the two diabatic components of the wavepacket and only accounts for the phase difference accumulated during the dynamics. In particular, $\mathcal{O}_{Q/A}^{Q+A}(0)$ are always real-valued and $\mathcal{O}^{Q+A}(0)$ is equal to 1, regardless of the initial phases. Figure 5 reports the phase difference, $\Delta\varphi(t)$, after initial excitation of $\frac{1}{\sqrt{2}}(\Psi_Q + \Psi_A)$ in BZ (dashed) and FBZ (plain). Similar plots are reported as Fig. 11 in the SI for a series of initial phases between the diabatic states in equally weighted FBZ wavepackets.

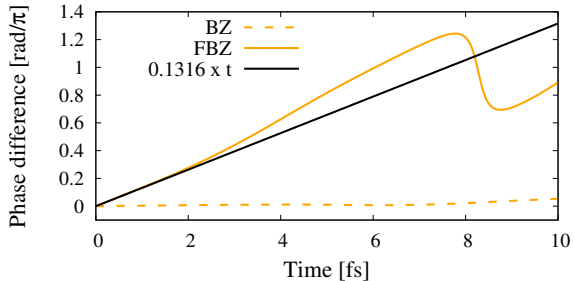


FIG. 5: Phase difference $\Delta\varphi$ between the diabatic components of the BZ (dashed) and FBZ (plain) autocorrelation functions upon population of $\frac{1}{\sqrt{2}}(\Psi_Q + \Psi_A)$. We also report the $0.1316 \times t$ line (black).

Formally, each diabatic component can be expanded in the adiabatic basis. In the present case, near the vertical ionization geometry, both Ψ_Q and Ψ_A are very strongly dominated by a single adiabatic state (more than 90% of their total norm). Therefore, the phase difference accumulated over a short period of τ a.u. is approximately $\tau \times \Delta E_{\text{vert}}$. In FBZ, the initial ≈ 0.27 eV gap should lead to a phase difference that accumulates at a rate of about $0.1316 \times \pi$ rad/fs (black line in Fig. 5).

In FBZ, Figure 5 clearly illustrates that the phase difference initially accumulates at the expected rate. The short time acceleration of the phase difference accumulation is explained by the system moving further away from the conical intersection therefore increasing the electronic energy gap. Notably, a phase difference of π , that maximizes interference effects, is reached just before 6 fs which corresponds to the time at which the full autocorrelation function presents a minimum (orange curve in Fig. 4). In the case of BZ, being restricted initially to a pure adiabatic state, the phase difference between the two diabatic components of the autocorrelation function accumulated throughout the dynamics remains extremely small. In this case, the vertical ionization geometry corresponds to the conical intersection, and thus the rate at which the phase difference is expected to accumulate is null. Obviously, the molecular wavepacket is not fully localised on the conical intersection and spreads and moves with time in non-degenerate regions, explaining the slight phase difference accumulated during the dynamics. However, subsequent interference effects remain fairly negligible.

Following the inter-state interference driven local minimum of $|\mathcal{O}^{Q+A}(t)|$, a small increase in its value can be observed. This originates from the diabatic component of the autocorrelation function with respect to the anti-quinoid state (dashed blue curve in Fig. 4) almost reaching zero around the 8.5 fs mark. With the cancellation of $\mathcal{O}_A^{Q+A}(t)$, the inter-state interference that causes the enhanced decay

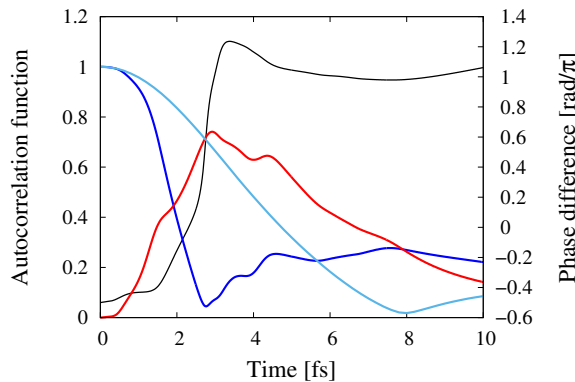


FIG. 6: Modulus of $\mathcal{O}^A(t)$ the autocorrelation function of the FBZ cation upon initial population of the pure Ψ_A diabatic state (light blue) and of its two space-restricted components $\mathcal{O}_+^A(t)$ (blue) and $\mathcal{O}_-^A(t)$ (red). Phase difference between the two space-restricted components of the autocorrelation function (black).

of the autocorrelation function is suppressed, leading to the slight revival in the autocorrelation function observed at later time. The near-cancellation of this term is also accompanied by a clear drop in the phase difference $\Delta\varphi(t)$ (Fig. 5). As demonstrated in SI (see Fig. 12), this sudden jump in the inter-state phase difference stems from a temporary but important change in the rate at which the phase of the antiquinoid component $\mathcal{O}_A^{Q+A}(t)$ accumulates over time.

As highlighted before, in this specific case, the $\mathcal{O}_A^{Q+A}(t)$ term displays a very similar behavior than $\mathcal{O}^A(t)$, the full autocorrelation function of the FBZ cation upon excitation to the pure Ψ_A diabatic state. Moreover, since, contrary to the $\mathcal{O}_A^{Q+A}(t)$ diabatic component, the full autocorrelation function $\mathcal{O}^A(t)$ is an experimental observable, we analyse in detail this case instead.

One of the reasons for the important decay of $\mathcal{O}^A(t)$ is the large diabatic population transfer at longer times (final quinoid population ≈ 0.46). This explains, in particular, the direction reversal of the average nuclear motion along the gradient difference vector observed in the right panel of Fig. 2. However, this large diabatic population transfer alone does not explain the full structure of $\mathcal{O}^A(t)$. Indeed, the simulation reveals that the near cancellation of $\mathcal{O}^A(t)$ around 8 fs is also driven by interference albeit, this time, involving different spatial components of the molecular wavepacket belonging to the Ψ_A diabatic state. This effect is named *intra-state interference* hereafter.

Figure 6 reports the autocorrelation function of the FBZ cation upon initial population of the pure Ψ_A diabatic state and its spatial restriction to the region of the space on either side of the conical intersection seam. More precisely, it is decomposed as

$$\mathcal{O}^A(t) = \mathcal{O}_+^A(t) + \mathcal{O}_-^A(t). \quad (4)$$

where $\mathcal{O}_+^A(t)$ and $\mathcal{O}_-^A(t)$ are computed by only accounting for GBF whose final position are either, on the same side of the conical intersection seam as the vertical ionization geometry *i.e.* $E_A^{\text{diab.}} - E_Q^{\text{diab.}} > 0$ (\mathcal{O}_+^A , blue), or on the opposite side: $E_A^{\text{diab.}} - E_Q^{\text{diab.}} < 0$ (\mathcal{O}_-^A , red). More information about this partitioning can be found in SI. The near cancellation of $\mathcal{O}^A(t)$ clearly stems from destructive intra-state interference between the space-restricted components $\mathcal{O}_+^A(t)$ and $\mathcal{O}_-^A(t)$: around the 8 fs mark, both components are characterized by equal modulus but with a phase difference (black) of about π radian, yielding almost total destructive intra-state interference.

In summary, upon ionization of the FBZ molecule, the autocorrelation function displays clear signature of the nature of the initially excited electronic wavepacket. This is in stark contrast with the case of the BZ molecule, due to the FBZ neutral geometry being displaced from the cationic conical intersection. In the latter case, different types of interference effects come into play. In particular, inter-state interference between the two diabatic components of the autocorrelation function leads to its accelerated decay upon excitation of a mixed electronic wavepacket. Also, at a later time of the dynamics, a different type of interference, this time of intra-state character, leads to the almost cancellation of the autocorrelation function of the FBZ cation upon population of the pure higher lying diabatic state. In particular, this is due to the destructive interference between the component of the autocorrelation function involving the part of the wavepacket that crosses the conical intersection seam during the dynamics and the part that ultimately remains on the same side as the vertical ionization geometry. The autocorrelation function being an experimentally measurable quantity, the identification of the predicted features in the autocorrelation functions of FBZ would thus be a clear observation of, not only the ability to control the induced molecular dynamics through the modulation of the populated wavepacket, but also of the coherent behavior and interference effects that drives it. We hope that the present study will motivate experimental studies of such quantum ultrafast dynamical effects.

Acknowledgments

We thank the *Région des Pays de la Loire* who provided post-doctoral funding for A.F. This work was performed using HPC resources from GENCI-IDRIS (Grant 101353) and CCIPL (Le centre de calcul intensif des Pays de la Loire).

[1] M. Hentschel, R. Kienberger, C. Spielmann, G. A. Reider, N. Milosevic, T. Brabec, P. Corkum, U. Heinzmann, M. Drescher, and F. Krausz, “Attosecond metrology,” *Nature*, vol. 414, no. 6863, pp. 509–513, 2001.

[2] P. M. Paul, E. S. Toma, P. Breger, G. Mullot, F. Augé, P. Balcou, H. G. Muller, and P. Agostini, “Observation of a train of attosecond pulses from high harmonic generation,” *Science*, vol. 292, no. 5522, pp. 1689–1692, 2001.

[3] F. Calegari, D. Ayuso, A. Trabattoni, L. Belshaw, S. De Camillis, S. Anumula, F. Frassetto, L. Poletto, A. Palacios, P. Decleva, J. B. Greenwood, F. Martín, and M. Nisoli, “Ultrafast electron dynamics in phenylalanine initiated by attosecond pulses,” *Science*, vol. 346, no. 6207, pp. 336–339, 2014.

[4] P. M. Kraus, B. Mignolet, D. Baykusheva, A. Rupenyan, L. Horný, E. F. Penka, G. Grassi, O. I. Tolstikhin, J. Schneider, F. Jensen, L. B. Madsen, A. D. Bandrauk, F. Remacle, and H. J. Wörner, “Measurement and laser control of attosecond charge migration in ionized iodoacetylene,” *Science*, vol. 350, no. 6262, pp. 790–795, 2015.

[5] T. Barillot, O. Alexander, B. Cooper, T. Driver, D. Garratt, S. Li, A. Al Haddad, A. Sanchez-Gonzalez, M. Agåker, C. Arrell, M. J. Bearpark, N. Berrah, C. Bostedt, J. Bozek, C. Brahms, P. H. Bucksbaum, A. Clark, G. Doumy, R. Feifel, L. J. Frasinski, S. Jarosch, A. S. Johnson, L. Kjellsson, P. Kolorenč, Y. Kumagai, E. W. Larsen, P. Matia-Hernando, M. Robb, J.-E. Rubensson, M. Ruberti, C. Sathe, R. J. Squibb, A. Tan, J. W. G. Tisch, M. Vacher, D. J. Walke, T. J. A. Wolf, D. Wood, V. Zhaunerchyk, P. Walter, T. Osipov, A. Marinelli, T. J. Maxwell, R. Coffee, A. A. Lutman, V. Averbukh, K. Ueda, J. P. Cryan, and J. P. Marangos, “Correlation-driven transient hole dynamics resolved in space and time in the isopropanol molecule,” *Phys. Rev. X*, vol. 11, p. 031048, Sep 2021.

[6] E. P. Måansson, S. Latini, F. Covito, V. Wanie, M. Galli, E. Perfetto, G. Stefanucci, H. Hübener, U. De Giovannini, M. C. Castrovilli, A. Trabattoni, F. Frassetto, L. Poletto, J. B. Greenwood, F. Légaré, M. Nisoli, A. Rubio, and F. Calegari, “Real-time observation of a correlation-driven sub 3 fs charge migration in ionised adenine,” *Communications Chemistry*, vol. 4, no. 1, p. 73, 2021.

[7] L. Cederbaum and J. Zobeley, “Ultrafast charge migration by electron correlation,” *Chemical Physics Letters*, vol. 307, no. 3–4, pp. 205 – 210, 1999.

[8] F. Remacle and R. D. Levine, “An electronic time scale in chemistry,” *Proceedings of the National Academy of Sciences*, vol. 103, no. 18, pp. 6793–6798, 2006.

[9] M. Nisoli, P. Decleva, F. Calegari, A. Palacios, and F. Martín, “Attosecond electron dynamics in molecules,” *Chemical Reviews*, vol. 0, no. 0, p. null, 0.

[10] V. Roudnev, B. D. Esry, and I. Ben-Itzhak, “Controlling hd^+ and h_2^+ dissociation with the carrier-envelope phase difference of an intense ultrashort laser pulse,” *Phys. Rev. Lett.*, vol. 93, p. 163601, Oct 2004.

[11] M. F. Kling, C. Siedschlag, A. J. Verhoef, J. I. Khan, M. Schultze, T. Uphues, Y. Ni, M. Uiberacker, M. Drescher, F. Krausz, and M. J. J. Vrakking, “Control of electron localization in molecular dissociation,” *Science*, vol. 312, no. 5771, pp. 246–248, 2006.

[12] I. C. D. Merritt, D. Jacquemin, and M. Vacher, “Attochemistry: Is controlling electrons the future of photochemistry?,” *The Journal of Physical Chemistry Letters*, vol. 12, no. 34, pp. 8404–8415, 2021. PMID: 34436903.

[13] A. Ferté and M. Vacher, “Recent advances in theoretical attosecond chemistry.” Published as Chapter 5 in *Chemical Modelling: Volume 17*, edited by H. Bahmann and J. C. Tremblay (RSC Publishing), :153–178, 2022.

[14] J. C. Travers, T. F. Grigorova, C. Brahms, and F. Belli, “High-energy pulse self-compression and ultraviolet generation through soliton dynamics in hollow capillary fibres,” *Nature Photonics*, vol. 13, no. 8, pp. 547–554, 2019.

[15] J. Duris, S. Li, T. Driver, E. G. Champenois, J. P. MacArthur, A. A. Lutman, Z. Zhang, P. Rosenberger, J. W. Aldrich, R. Coffee, G. Coslovich, F.-J. Decker, J. M. Gownia, G. Hartmann, W. Helml, A. Kamalov, J. Knurr, J. Krzywinski, M.-F. Lin, J. P. Marangos, M. Nantel, A. Natan, J. T. O’Neal, N. Shivaram, P. Walter, A. L. Wang, J. J. Welch, T. J. A. Wolf, J. Z. Xu, M. F. Kling, P. H. Bucksbaum, A. Zholents, Z. Huang, J. P. Cryan, and A. Marinelli, “Tunable isolated attosecond x-ray pulses with gigawatt peak power from a free-electron laser,” *Nature Photonics*, vol. 14, no. 1, pp. 30–36, 2020.

[16] J. T. O’Neal, E. G. Champenois, S. Oberli, R. Obaid, A. Al-Haddad, J. Barnard, N. Berrah, R. Coffee, J. Duris, G. Galinis, D. Garratt, J. M. Gownia, D. Haxton, P. Ho, S. Li, X. Li, J. MacArthur, J. P. Marangos, A. Natan, N. Shivaram, D. S. Slaughter, P. Walter, S. Wandel, L. Young, C. Bostedt, P. H. Bucksbaum, A. Picón, A. Marinelli, and J. P. Cryan, “Electronic population transfer via impulsive stimulated x-ray raman scattering with attosecond soft-x-ray pulses,” *Phys. Rev. Lett.*, vol. 125, p. 073203, Aug 2020.

[17] M. Kretschmar, A. Hadjipittas, B. Major, J. Tümmler, I. Will, T. Nagy, M. J. J. Vrakking, A. Emmanouilidou, and B. Schütte, “Attosecond investigation of extreme-ultraviolet multi-photon multi-electron ionization,” *Optica*, vol. 9, pp. 639–644, Jun 2022.

[18] J. P. Marangos, “Development of high harmonic generation spectroscopy of organic molecules and biomolecules,” *Journal of Physics B: Atomic, Molecular and Optical Physics*, vol. 49, p. 132001, may 2016.

[19] Y. Mairesse, A. de Bohan, L. J. Frasinski,

H. Merdji, L. C. Dinu, P. Monchicourt, P. Breger, M. Kovačev, R. Taïeb, B. Carré, H. G. Muller, P. Agostini, and P. Salières, “Attosecond synchronization of high-harmonic soft x-rays,” *Science*, vol. 302, no. 5650, pp. 1540–1543, 2003.

[20] M. Lein, “Attosecond probing of vibrational dynamics with high-harmonic generation,” *Phys. Rev. Lett.*, vol. 94, p. 053004, Feb 2005.

[21] S. Baker, J. S. Robinson, C. A. Haworth, H. Teng, R. A. Smith, C. C. Chirilă, M. Lein, J. W. G. Tisch, and J. P. Marangos, “Probing proton dynamics in molecules on an attosecond time scale,” *Science*, vol. 312, no. 5772, pp. 424–427, 2006.

[22] J. P. Farrell, S. Petretti, J. Förster, B. K. McFarland, L. S. Spector, Y. V. Vanne, P. Decleva, P. H. Bucksbaum, A. Saenz, and M. Gühr, “Strong field ionization to multiple electronic states in water,” *Phys. Rev. Lett.*, vol. 107, p. 083001, Aug 2011.

[23] Z. Diveki, A. Camper, S. Haessler, T. Auguste, T. Ruchon, B. Carré, P. Salières, R. Guichard, J. Caillat, A. Maquet, and R. Taïeb, “Spectrally resolved multi-channel contributions to the harmonic emission in n2,” *New Journal of Physics*, vol. 14, p. 023062, feb 2012.

[24] P. M. Kraus and H. J. Wörner, “Attosecond nuclear dynamics in the ammonia cation: Relation between high-harmonic and photoelectron spectroscopies,” *ChemPhysChem*, vol. 14, no. 7, pp. 1445–1450, 2013.

[25] P. Lan, M. Ruhmann, L. He, C. Zhai, F. Wang, X. Zhu, Q. Zhang, Y. Zhou, M. Li, M. Lein, and P. Lu, “Attosecond probing of nuclear dynamics with trajectory-resolved high-harmonic spectroscopy,” *Phys. Rev. Lett.*, vol. 119, p. 033201, Jul 2017.

[26] C. E. M. Gonçalves, R. D. Levine, and F. Remacle, “Ultrafast geometrical reorganization of a methane cation upon sudden ionization: an isotope effect on electronic non-equilibrium quantum dynamics,” *Phys. Chem. Chem. Phys.*, vol. 23, pp. 12051–12059, 2021.

[27] D. R. Austin, A. S. Johnson, F. McGrath, D. Wood, L. Miseikis, T. Siegel, P. Hawkins, A. Harvey, Z. Maśn, S. Patchkovskii, M. Vacher, J. P. Malhado, M. Y. Ivanov, O. Smirnova, and J. P. Marangos, “Extracting sub-cycle electronic and nuclear dynamics from high harmonic spectra,” *Scientific Reports*, vol. 11, no. 1, p. 2485, 2021.

[28] A. Nikodem, R. D. Levine, and F. Remacle, “Spatial and temporal control of populations, branching ratios, and electronic coherences in lih by a single one-cycle infrared pulse,” *Phys. Rev. A*, vol. 95, p. 053404, May 2017.

[29] T. Schnappinger and R. de Vivie-Riedle, “Coupled nuclear and electron dynamics in the vicinity of a conical intersection,” *J. Chem. Phys.*, vol. 154, no. 13, p. 134306, 2021.

[30] F. Schüppel, T. Schnappinger, L. Bäuml, and R. de Vivie-Riedle, “Waveform control of molecular dynamics close to a conical intersection,” *J. Chem. Phys.*, vol. 153, no. 22, p. 224307, 2020.

[31] A. Valentini, S. van den Wildenberg, and F. Remacle, “Selective bond formation triggered by short optical pulses: quantum dynamics of a four-center ring closure,” *Phys. Chem. Chem. Phys.*, vol. 22, pp. 22302–22313, 2020.

[32] J. Meisner, M. Vacher, M. J. Bearpark, and M. A. Robb, “Geometric rotation of the nuclear gradient at a conical intersection: Extension to complex rotation of diabatic states,” *Journal of Chemical Theory and Computation*, vol. 11, no. 7, pp. 3115–3122, 2015. PMID: 26575748.

[33] M. Vacher, F. E. A. Albertani, A. J. Jenkins, I. Polyak, M. J. Bearpark, and M. A. Robb, “Electron and nuclear dynamics following ionisation of modified bismethylene-adamantane,” *Faraday Discuss.*, vol. 194, pp. 95–115, 2016.

[34] T. Tran, G. A. Worth, and M. A. Robb, “Control of nuclear dynamics in the benzene cation by electronic wavepacket composition,” *Communications Chemistry*, vol. 4, no. 1, p. 48, 2021.

[35] D. Danilov, T. Tran, M. J. Bearpark, J. P. Marangos, G. A. Worth, and M. A. Robb, “How electronic superpositions drive nuclear motion following the creation of a localized hole in the glycine radical cation,” *The Journal of Chemical Physics*, vol. 156, 06 2022. 244114.

[36] M. Vacher, D. Mendive-Tapia, M. J. Bearpark, and M. A. Robb, “Electron dynamics upon ionization: Control of the timescale through chemical substitution and effect of nuclear motion,” *The Journal of Chemical Physics*, vol. 142, no. 9, pp. –, 2015.

[37] V. Despré, A. Marciniak, V. Loriot, M. C. E. Galbraith, A. Rouzée, M. J. J. Vrakking, F. Lépine, and A. I. Kuleff, “Attosecond hole migration in benzene molecules surviving nuclear motion,” *The Journal of Physical Chemistry Letters*, vol. 6, no. 0, pp. 426–431, 2015.

[38] T. K. Kjeldsen, C. Z. Bisgaard, L. B. Madsen, and H. Stapelfeldt, “Role of symmetry in strong-field ionization of molecules,” *Phys. Rev. A*, vol. 68, p. 063407, Dec 2003.

[39] T. K. Kjeldsen, C. Z. Bisgaard, L. B. Madsen, and H. Stapelfeldt, “Influence of molecular symmetry on strong-field ionization: Studies on ethylene, benzene, fluorobenzene, and chlorofluorobenzene,” *Phys. Rev. A*, vol. 71, p. 013418, Jan 2005.

[40] M. Vacher, L. Steinberg, A. J. Jenkins, M. J. Bearpark, and M. A. Robb, “Electron dynamics following photoionization: Decoherence due to the nuclear-wave-packet width,” *Phys. Rev. A*, vol. 92, p. 040502, Oct 2015.

[41] M. Vacher, M. J. Bearpark, M. A. Robb, and J. a. P. Malhado, “Electron dynamics upon ionization of polyatomic molecules: Coupling to quantum nuclear motion and decoherence,” *Phys. Rev. Lett.*, vol. 118, p. 083001, Feb 2017.

[42] C. Arnold, O. Vendrell, and R. Santra, “Electronic decoherence following photoionization: Full quantum-dynamical treatment of the influence of nuclear motion,” *Phys. Rev. A*, vol. 95, p. 033425, Mar 2017.

[43] V. Despré, N. V. Golubev, and A. I. Kuleff, “Charge migration in propionic acid: A full quantum dynamical study,” *Phys. Rev. Lett.*, vol. 121, p. 203002, Nov 2018.

[44] C. Arnold, C. Larivière-Loiselle, K. Khalili, L. Inhester, R. Welsch, and R. Santra, “Molecular

electronic decoherence following attosecond photoionisation,” *J. Phys. B: At. Mol. Opt.*, vol. 53, p. 164006, jun 2020.

[45] N. V. Golubev, T. Begušić, and J. Vaníček, “On-the-fly ab initio semiclassical evaluation of electronic coherences in polyatomic molecules reveals a simple mechanism of decoherence,” *Phys. Rev. Lett.*, vol. 125, p. 083001, Aug 2020.

[46] D. T. Matselyukh, V. Despré, N. V. Golubev, A. I. Kuleff, and H. J. Wörner, “Decoherence and revival in attosecond charge migration driven by non-adiabatic dynamics,” *Nature Physics*, vol. 18, no. 10, pp. 1206–1213, 2022.

[47] D. Dey, A. I. Kuleff, and G. A. Worth, “Quantum interference paves the way for long-lived electronic coherences,” *Phys. Rev. Lett.*, vol. 129, no. 17, p. 173203, 2022.

[48] M. Vacher, J. Meisner, D. Mendive-Tapia, M. J. Bearpark, and M. A. Robb, “Electronic control of initial nuclear dynamics adjacent to a conical intersection,” *The Journal of Physical Chemistry A*, vol. 119, no. 21, pp. 5165–5172, 2015. PMID: 25466408.

[49] G. Worth, “Quantics: A general purpose package for quantum molecular dynamics simulations,” *Comput. Phys. Commun.*, vol. 248, p. 107040, 2020.

[50] G. A. Worth and I. Burghardt, “Full quantum mechanical molecular dynamics using gaussian wavepackets,” *Chemical Physics Letters*, vol. 368, no. 3–4, pp. 502 – 508, 2003.

[51] G. Richings, I. Polyak, K. Spinlove, G. Worth, I. Burghardt, and B. Lasorne, “Quantum dynamics simulations using gaussian wavepackets: the vmcg method,” *International Reviews in Physical Chemistry*, vol. 34, no. 2, pp. 269–308, 2015.

[52] M. Vacher, M. J. Bearpark, and M. A. Robb, “Direct methods for non-adiabatic dynamics: connecting the single-set variational multi-configuration gaussian (vmcg) and ehrenfest perspectives,” *Theoretical Chemistry Accounts*, vol. 135, no. 8, pp. 1–11, 2016.

[53] M. J. Frisch, G. W. Trucks, H. B. Schlegel, G. E. Scuseria, M. A. Robb, J. R. Cheeseman, G. Scalmani, V. Barone, G. A. Petersson, H. Nakatsuji, X. Li, M. Caricato, A. V. Marenich, J. Bloino, B. G. Janesko, R. Gomperts, B. Mennucci, H. P. Hratchian, J. V. Ortiz, A. F. Izmaylov, J. L. Sonnenberg, D. Williams-Young, F. Ding, F. Lipparini, F. Egidi, J. Goings, B. Peng, A. Petrone, T. Henderson, D. Ranasinghe, V. G. Zakrzewski, J. Gao, N. Rega, G. Zheng, W. Liang, M. Hada, M. Ehara, K. Toyota, R. Fukuda, J. Hasegawa, M. Ishida, T. Nakajima, Y. Honda, O. Kitao, H. Nakai, T. Vreven, K. Throssell, J. A. Montgomery, Jr., J. E. Peralta, F. Ogliaro, M. J. Bearpark, J. J. Heyd, E. N. Brothers, K. N. Kudin, V. N. Staroverov, T. A. Keith, R. Kobayashi, J. Normand, K. Raghavachari, A. P. Rendell, J. C. Burant, S. S. Iyengar, J. Tomasi, M. Cossi, J. M. Millam, M. Klene, C. Adamo, R. Cammi, J. W. Ochterski, R. L. Martin, K. Morokuma, O. Farkas, J. B. Foresman, and D. J. Fox, “Gaussian~16 Revision C.01,” 2016. Gaussian Inc. Wallingford CT.

[54] A. Thiel and H. Köppel, “Proposal and numerical test of a simple diabatization scheme,” *J. Chem. Phys.*, vol. 110, no. 19, pp. 9371–9383, 1999.

[55] H. Köppel, J. Gronki, and S. Mahapatra, “Construction scheme for regularized diabatic states,” *J. Chem. Phys.*, vol. 115, no. 6, pp. 2377–2388, 2001.

[56] C. Arnold, O. Vendrell, R. Welsch, and R. Santra, “Control of nuclear dynamics through conical intersections and electronic coherences,” *Phys. Rev. Lett.*, vol. 120, p. 123001, Mar 2018.

[57] S. Patchkovskii and M. S. Schuurman, “Short-time dynamics at a conical intersection in high-harmonic spectroscopy,” *The Journal of Physical Chemistry A*, vol. 118, no. 51, pp. 12069–12079, 2014. PMID: 25314638.

Supplementary materials

Illustration of the branching space vectors

Figure 7 presents a schematic representation of the gradient difference and derivative coupling vectors that define the branching space associated with the conical intersection between the quinoid and anti-quinoid cationic states of BZ and FBZ.

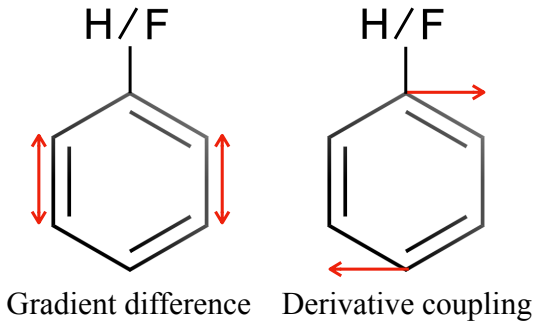


FIG. 7: Schematic representation of branching space vectors of the benzene and fluoro-benzene cations.

Convergence of the DD-vMCG dynamics

In order to asses the convergence of the DD-vMCG simulations, the number of GBF is increased until stabilization of the autocorelation functions. Figure 8 reports, as an example, the autocorrelation function computed along the dynamics of the FBZ cation upon initial population of the $\frac{1}{\sqrt{2}}(\Psi_Q + \Psi_A)$ wavepacket and for different number of GBF. As one can see, both orange and black curves, respectively obtained with 10 and 15 GBF, are superimposed.

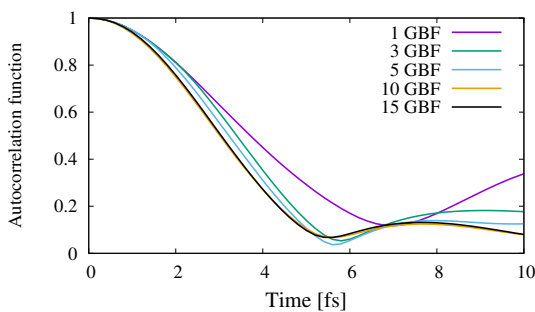


FIG. 8: Modulus of $\mathcal{O}^{Q+A}(t)$ the autocorrelation function of FBZ upon initial population of the $\frac{1}{\sqrt{2}}(\Psi_Q + \Psi_A)$ cationic wavepacket during the DD-vMCG dynamics simulation: 1 GBF (purple), 3 GBF (green), 5 GBF (blue), 10 GBF (orange), and 15 GBF (black).

BZ and deuterated BZ dynamics

In figure 9, we compare the dynamics of the BZ and deuterated benzene (DBZ) cation upon population of Ψ_Q (purple), Ψ_A (blue), $\frac{1}{\sqrt{2}}(\Psi_Q + \Psi_A)$ (orange) and $\frac{1}{\sqrt{2}}(\Psi_Q - \Psi_A)$ (green) wave packets. As one can see, since the induced nuclear motion do not significantly involve the carbon-hydrogen or carbon-deuterium bonds, both molecules yields fairly similar dynamics.

Diabatic decomposition of the autocorelation function of BZ and FBZ mixed wavepackets

Figure 10 shows similar diabatic decompositions of the autocorrelation functions (as reported in the main text of this letter) for both $\frac{1}{\sqrt{2}}(\Psi_Q \pm \Psi_A)$ mixed wavepackets and for both BZ (right) and FBZ (left) molecules. Clearly, there is no inter-state interference effects in the case of BZ contrary to the FBZ case. Indeed, in the former case, the modulus of the full autocorrelation function (black) is equal to the incoherent sum of the modulus of the two diabatic components (grey). As thoroughly discussed in the main body of this letter, this is not the case for FBZ. Moreover, this figure illustrates the symmetry that exists between both in phase (top row) and opposite phase (bottom) wavepackets due to the symmetry of the system with respect to the molecular displacement along the derivative coupling vector. Indeed, for both systems, despite leading to molecular displacement in opposite direction with respect to the derivative coupling vector, both wavepackets yields indistinguishable autocorrelation functions.

Independence of the inter-state interference effects to the initial phases of the diabatic components of the wavepacket

As stated in the main body of this letter, the inter-state interference effects observed in case of a mixed cationic wavepacket of FBZ are independent of the absolute and relative phases of the diabatic components of the initial wavepacket. To illustrate this property, the left panel of figure 11 reports the modulus of the autocorrelation function of the FBZ cation upon initial population of equally weighted wavepacket of the following form, $\frac{1}{\sqrt{2}}(\Psi_Q + \Psi_A e^{i\Delta\phi})$, for a series of initial electronic phase differences $\Delta\phi$. The right panel of figure 11 also reports the phase difference $\Delta\varphi$ between the two diabatic components of the autocorrelation function. As one can see, modulating the initial relative phases $\Delta\phi$ do not yield any modification of the subsequent autocorrelation function.

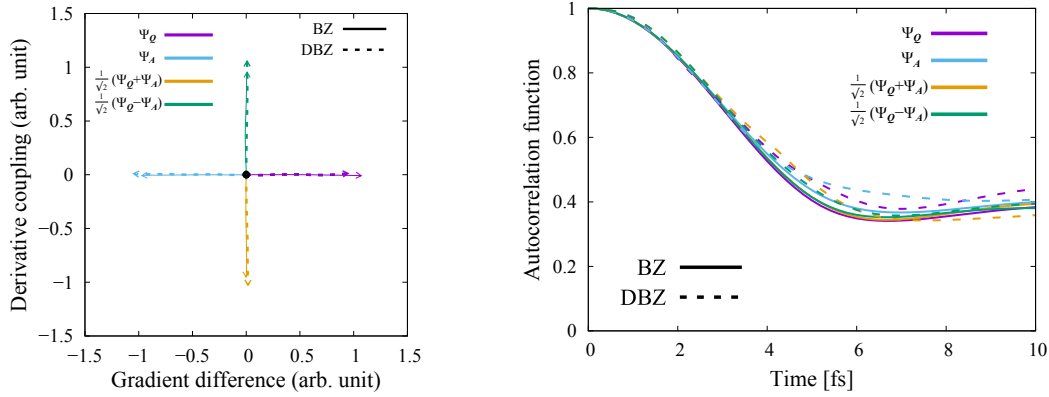


FIG. 9: Left: Average quantum nuclear motion in the branching space over 10 fs and upon ionization of BZ (plain) and DBZ (dashed) cation upon initial population of Ψ_Q (purple), Ψ_A (blue), $\frac{1}{\sqrt{2}}(\Psi_Q + \Psi_A)$ (orange) and $\frac{1}{\sqrt{2}}(\Psi_Q - \Psi_A)$ (green). Right: Modulus of the autocorrelation functions along the quantum dynamics induced upon ionization of BZ (plain) and DBZ (dashed) molecules and excitation to Ψ_Q (purple), Ψ_A (blue), $\frac{1}{\sqrt{2}}(\Psi_Q + \Psi_A)$ (orange) and $\frac{1}{\sqrt{2}}(\Psi_Q - \Psi_A)$ (green) electronic wavepackets.

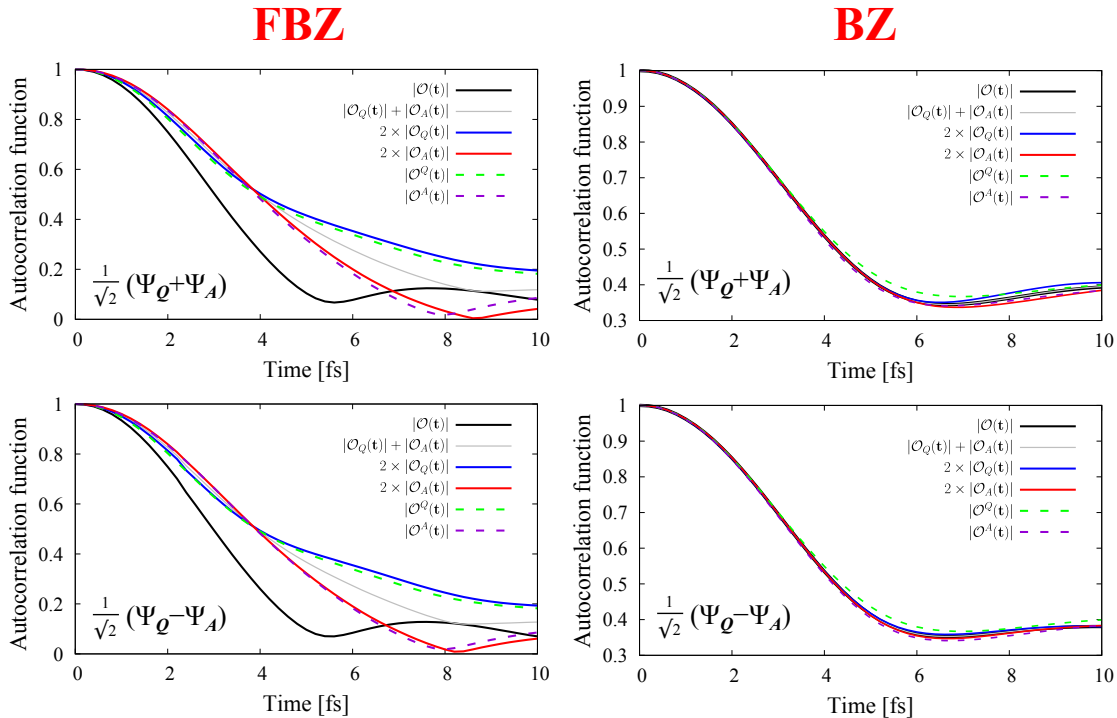


FIG. 10: Modulus of the autocorrelation functions of the FBZ (left) and BZ (right) cations upon initial population of an equally weighted superposition of the two diabatic states (black). The initial composition of the wavepacket is reported in the bottom left corners of each figures. Diabatic components of the full autocorrelation function, $\mathcal{O}_Q(t)$ (blue) and $\mathcal{O}_A(t)$ (red), note that they were doubled here for ease of representation. Incoherent sum $|\mathcal{O}_Q(t)| + |\mathcal{O}_A(t)|$ (grey). Modulus of the autocorrelation functions of the cations upon initial population of a pure diabatic state, $\mathcal{O}^Q(t)$ (dashed green) and $\mathcal{O}^A(t)$ (dashed purple).

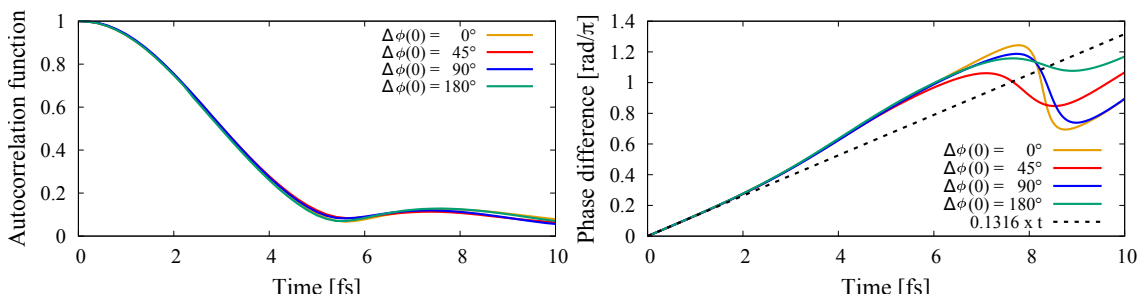


FIG. 11: Upon population of an equally weighted superposition of the two diabatic states of the FBZ molecule with

Phase accumulation rate of the diabatic components of the autocorelation function

Figure 12 reports the derivative with respect to time of the phase of each diabatic components of the full autocorrelation function of the FBZ cation upon initial excitation of the $\frac{1}{\sqrt{2}}(\Psi_Q + \Psi_A)$ wavepacket. This figure clearly illustrates that the phase of the $\mathcal{O}_Q^{Q+A}(t)$ term accumulates quasi linearly with time while the $\mathcal{O}_A^{Q+A}(t)$ term presents an important variation of its accumulation rate over a short time period around 7.5 to 9.0 fs. As stated in the main body of this letter, this variation in the time derivative of the phase of $\mathcal{O}_A^{Q+A}(t)$ leads to the step-like feature observed in the evolution of the $\Delta\varphi$ phase difference.

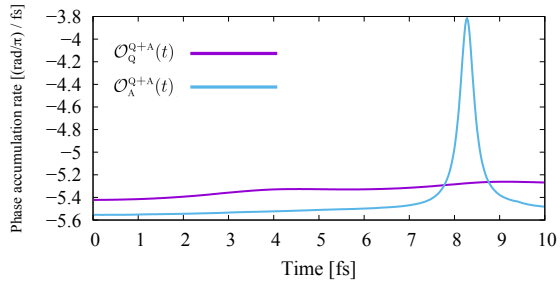


FIG. 12: Time derivative of the phase of the diabatic components of the full FBZ cation autocorrelation function upon excitation to the $\frac{1}{\sqrt{2}}(\Psi_Q + \Psi_A)$ wavepacket. Purple: Time derivative of the complex phase of $\mathcal{O}_Q^{Q+A}(t)$. Blue: Time derivative of the complex phase of $\mathcal{O}_A^{Q+A}(t)$.

Spatial partition of the autocorrelation function

The partitioning of the full autocorrelation function of the FBZ cation upon initial population of the anti-quinoid diabatic state, in the two $\mathcal{O}_+^A(t)$ and $\mathcal{O}_-^A(t)$ space restricted components was obtained by only accounting for the GBF whose final positions are on a given side of the conical intersection seam. This decomposition is motivated by the results displayed in Fig. 13 and 14. The former shows the trajectory in the branching plane of each GBF during the dynamics induced upon population of Ψ_A . On the other hand, the later shows the diabatic energy gap at the position of each GBF centers. The GBF partitioning used in the decomposition of the autocorrelation function is depicted by the color coding in these figures.

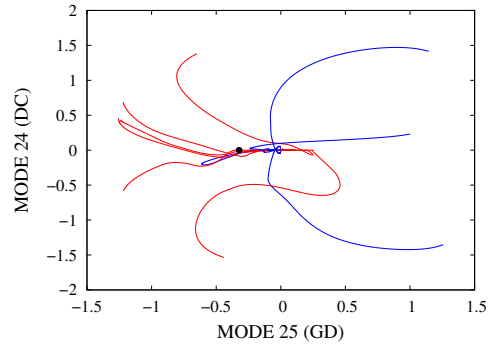


FIG. 13: Trajectory, in the plane spanned by the vector of the normal mode 24 (representative of the DC) and 25 (representative of the GD), of the 10 GBF during the DD-vMCG simulation of the non-adiabatic dynamics of the FBZ cation upon initial excitation of the pure Ψ_A diabatic state. The color coding is used to highlight similar behavior within the GBF trajectories.

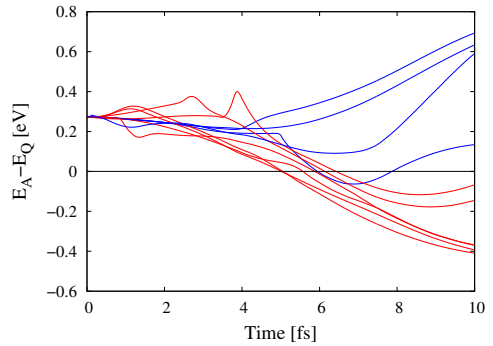


FIG. 14: Diabatic energy difference $E_A - E_Q$ at the position of each GBF center during the DD-vMCG simulation of the non-adiabatic dynamics of the FBZ cation upon initial excitation of the pure Ψ_A diabatic state. The color coding is used to highlight similar behavior within the GBF trajectories.